Assessment of the Mechanical Integrity and Feasibility of Hyper PLA-CF for High-Speed FDM Manufacturing of Functional Components

Roaa H. Ibrahim[1,*] and Hala Salman Hasan[2]

[1]University of Sumer, Al Nahrain University, College of Engineering, Mechanical Engineering Department

[2]Al Nahrain University, College of Engineering, Mechanical Engineering Department

Abstract: Fused Filament Fabrication (FFF), also known as Fused Deposition Modeling (FDM), has attracted considerable attention over the past decade due to rapid technological advancements that have enabled a transition from prototyping to the production of functional components. This research investigates the viability of next-generation composite materials for high-speed printing, a topic that is seldom studied. It emphasizes Hyper Polylactic Acid reinforced with Carbon Fiber (Hyper PLA-CF), engineered for high-speed printing, wherein increased printing speeds, accelerated cooling, and reduced polymer chain diffusion modify thermal and bonding properties beyond the capabilities of conventional PLA-CF. The study evaluates mechanical performance, including tensile, compressive, bending, and impact properties, in relation to printing parameters such as layer thickness, nozzle temperature, build plate temperature, and printing speed, utilizing Taguchi design, Multiple Linear Regression (MLR), and Analysis of Variance (ANOVA). Scanning Electron Microscope (SEM) analysis was employed to investigate the microstructural characteristics. The results demonstrate that Hyper PLA-CF maintains high strength at elevated speeds, with strength influenced by the interaction between thermal parameters and layer geometry. Layer thickness notably influences tensile, bending, and impact properties, whereas build plate temperature primarily affects compression strength. SEM observations confirmed the influence of layer thickness and nozzle temperature on interlayer bonding and failure modes. These findings establish design parameters for reliable high-speed FFF utilizing Hyper PLA-CF on the CREALITY K1C, thereby addressing a critical gap in industrial implementation.

Keywords: Additive manufacturing (AM), Fused Filament Fabrication (FFF), Fused Deposition Modeling (FDM), Hyper PLA-CF, Printing parameters, Mechanical performance, Microstructure Assessment.

1. INTRODUCTION

Fused Filament Fabrication (FFF) is a widely popular Additive manufacturing technique, valued for its affordability in fabricating complex geometries and its compatibility with numerous thermoplastic materials. Increasingly, FFF is being used to produce structural parts rather than only prototypes. While pure thermoplastics dominated in previous decades, the demand for enhanced mechanical performance has driven the development of composite materials. Polylactic acid (PLA), a biodegradable polymer, is commonly derived from renewable resources such as corn starch and cassava [1]. However, PLA exhibits limitations, including low thermal stability and brittleness, which restrict its mechanical performance and limit its use in manufacturing functional parts [1, 2]. The incorporation of carbon fiber reinforcement significantly enhances the tensile strength and dimensional stability of PLA-based composites, yielding materials with a high strength-to-weight ratio suitable for lightweight applications [3, 4].

Recent advancements have led to the development of specialized high-speed filaments, often referred to as ‘hyper-speed’, designed to complement a new generation of FFF printers capable of speeds exceeds 300mm/s [5]. Hyper PLA-CF, for instance, has been engineered to maintain part integrity and robust layer adhesion under these demanding high-speed printing conditions [6]. However, the rapid printing and subsequent cooling inherent in these processes introduce complex thermal behaviors that affect the crystallization and interlayer bonding between carbon fibers and the polymer matrix [7]. This highlights a key challenge: the speed-strength paradox within the FFF process. While elevating printing velocities enhances manufacturing throughput, it may undermine the mechanical integrity of the components owing to reduced thermal diffusion durations and modified interlayer adhesion [5]. Understanding this trade-off is crucial for producing functional components that require reliable mechanical performance under real-world loading conditions.

Recent advancements in FFF-printed polymer composites have been critically assessed in a previous review article authored by the present researchers [8]. FFF processing parameters have markedly impacted the microstructure and mechanical performance of FFF-printed components. These effects depend on the thermal history of the deposited material, which is directly influenced by nozzle temperature, build plate temperature, and printing speed. The present study

*Address correspondence to this author at the University of Sumer, Al Nahrain University, College of Engineering, Mechanical Engineering Department; E-mail: st.roaa.h.ibrahim@ced.nahrainuniv.edu.iq

Received on 03-06-2026 Accepted on 15-07-2026 Published on 22-07-2026

E-ISSN: 2311-8717/26

extends that work through experimental validation and provides a robust, comprehensive assessment of the mechanical performance of Hyper PLA-CF when processed via FFF at high speeds. The objective is to facilitate the industrial adoption of high-speed composite materials for manufacturing functional components via FFF. This study represents one phase of a broader investigation into the mechanical performance and optimization of FFF-printed carbon-fiber-reinforced thermoplastics.

An analysis of the existing research indicates that nearly all studies on PLA-CF parameters operate at conventional printing speeds substantially lower than those used in the present work: Wang *et al*. [9] optimized PLA with 5% Carbon Fiber composites at speeds with ranges (20-80 mm/s); Kamaal *et al*. [10] examined PLA with 5.50% CF at speeds up to 60 mm/s. The only study approaching the ultra-high-speed regime for PLA is by Farzipour and Hasanzadeh [5], who tested plain PLA at speeds up to 500 mm/s and limited their analysis to tensile behavior only. Blake *et al*. [11] focused on the effects of nozzle diameter on PLA containing approximately 15–20 wt.% carbon fiber.

Farj and Ahmed [6] examined carbon fiber-reinforced polylactic acid at various print speeds but limited their analysis to thermal, structural, and chemical characterization via differential scanning calorimetry, thermogravimetric analysis, X-ray diffraction, and Fourier transform infrared spectroscopy, without employing multimodal mechanical testing or Taguchi-based optimization. The only published study on the Hyper series filament was conducted by Kumaresan *et al*. [12] investigating Hyper PLA without carbon fiber at fixed process parameters, varying only the infill pattern and density, and did not address compressive or impact behavior. Consequently, to date, no study has provided a combined Taguchi-based parametric investigation and four-mode mechanical characterization (tensile, compressive, bending, and impact strength) of Hyper PLA-CF within the 200–300 mm/s speed range. This gap represents both a scientific deficiency and a practical barrier: engineers aiming to utilize Hyper PLA-CF for functional components currently lack validated process-property relationships at the operational speeds for which this material is specifically designed [13].

Prior studies have demonstrated that FFF printing parameters such as infill pattern, building orientation, printing speed, layer thickness, and nozzle temperature have a great impact on mechanical properties [11, 14]. Araque *et al*. [14] have examined the effect of printing angle and layer height on the mechanical performance of PLA-CF. Tensile and bending tests were conducted, and the findings indicate that both factors significantly influence mechanical strength. Printing at lower angles (0° and 15°) generally resulted in greater resistance under tension and bending, attributed to favorable fiber alignment and improved load distribution. Conversely, higher angles (60° to 90°) significantly diminished strength, with tensile failures due to delamination and bending forces as low as, thereby highlighting the vulnerability of perpendicular layer interfaces.

Mengyu Cao *et al*.[4] have examined the impact of carbon fiber on the tensile characteristics of polylactic acid (PLA). Their findings indicate that incorporating carbon fiber reduces the tensile strength of the PLA specimen from 54.51 MPa to 49.41 MPa relative to the pure PLA component. Conversely, the Young's modulus and the elongation-at-break of the PLA-CF specimen increased from 1.04 GPa and 6.26% to 1.26 GPa and 7.81%, respectively. The analysis of the results demonstrated that the fracture behavior of the PLA-CF specimen shifted from brittle to ductile following the integration of carbon fiber into the PLA matrix.

Ali *et al*. [2] have investigated the performance of both PLA and PLA-CF at varying infill densities. Tensile and Izod tests were conducted, and the results showed that tensile and impact strength increased with increasing infill density, and that PLA-CF has higher strength than PLA.

Kamaal *et al*. [10] also performed tensile and impact tests to examine the performance of PLA-CF regarding building direction, infill percentage, and layer height printing parameters. It was demonstrated that tensile properties were affected by all three factors; however, for infill percentage and layer height, there is a threshold beyond which the effects become significantly more pronounced than at lower values. The highest tensile strength was achieved with a layer height of 0.25 mm and an infill percentage of 80%. Concerning the Izod test results, it was observed that layer height has a minimal impact on strength, whereas building direction and infill percentage significantly influence it.

Andong Wang *et al*. [9] investigated the impact of FFF process parameters on the mechanical properties of PLA composites. The findings reveal that the incorporation of 5 wt.% CF significantly enhances the stiffness and overall mechanical characteristics of the PLA composite. The hierarchy of printing factors affecting the tensile strength of the PLA composite product is as follows: printing layer thickness, bottom plate temperature, printing speed, and nozzle temperature. Ultimately, the maximum tensile strength is achieved under specific conditions: a 0.1 mm layer thickness, a 60 ◦C bottom plate temperature, a 40 mm/s printing speed, and a 215 ◦C nozzle temperature.

Kumaresan *et al*. [12] examined the mechanical and microstructural aspects of Hyper-PLA by modifying the infill patterns and densities, while maintaining constant parameters such as layer thickness, raster angle, and printing speed. In this study, the mechanical characteristics of Hyper-PLA are analyzed through variations in infill pattern (Grid, Rectilinear, Honeycomb, Gyroid, Concentric) and infill density (50%, 75%, and 100%). The results clearly demonstrate that Hyper-PLA exhibits mechanical properties approximately 10–20% superior to those of PLA. The mechanical properties of the specimens increase with higher infill densities. Additionally, the infill patterns significantly influence the material properties.

Blake *et al*. [11] systematically examined the mechanical and microstructural behavior of FFF-printed PLA and PLA-CF composites, focusing on the effects of nozzle diameter and material composition. Tensile and flexural tests, along with cross-sectional imaging, were performed to investigate the microstructural mechanisms influencing mechanical performance. Results show that increasing nozzle diameter typically enhances both Ultimate Tensile Strength (UTS) and Ultimate Flexural Strength (UFS), with a more significant impact on flexural performance. The addition of carbon fibers improves stiffness and strength but also introduces challenges such as increased brittleness and uneven bead formation. Cross-sectional images reveal notable differences in porosity, inter-bead bonding, and filament shape among samples.

2. MATERIALS AND METHODS

2.1. Materials

Hyper PLA-CF, a commercially available filament from CREALITY, was dried prior to printing using a CREALITY dryer, as illustrated in Figure **1**(**a**). The Hyper PLA-CF filament depicted in Figure **1**(**b**) possesses physical properties, with the drying conditions summarized in Table **1**.

Table 1: Some properties of Hyper PLA-CF filament and drying conditions

Property of Filament	Value
Density	1.21 (g/mm3)
Diameter	1.75 (mm)
Carbon fiber	4 %
Drying conditions	50 °C, 6 h

2.2. Printing Parameters and Experimental Design (Taguchi)

A Design of Experiments (DoE) approach, specifically the Taguchi method, was used with Minitab Statistical Software (version 22) to plan the experimental runs. Four printing parameters, namely layer thickness, inner wall and sparse infill speed, nozzle temperature, and build plate temperature, were investigated, each at three levels. A full factorial design would require 81 experimental combinations (3^4 = 81 runs). To minimize the effort and maintain a balanced and statistically efficient design, the L9 Taguchi array was utilized, thereby reducing the number of runs from 81 to 9 runs. The four parameters with the three levels require 8 degrees of freedom [4 Factors* (3-1) Levels=8], which corresponds to the eight-degree freedom available in an L9 orthogonal array [9 (Number of runs)-1=8]. Table **2** presents the Taguchi L9 matrix, while other printing parameters, detailed in Table **3**, were carefully chosen to maximize the strength of the printed component, as their effects are well documented in the literature. Table **4** presents the levels of the printing parameters in the Taguchi L9 array.

Table 2: Key parameters of Hyper PLA-CF

Printing Parameter	Levels
Layer thickness (mm)	0.1, 0.2, 0.3
Inner wall and Sparse infill speed (mm/s)	200, 250, 300
Nozzle Temperature (˚C)	200, 215, 230
Building Plate Temperature (˚C)	50, 60, 70

2.3. Specimen Design, Fabrication, Testing, and SEM Assessment

The tensile, compression, bending, and flexural tests were conducted in accordance with ASTM standards. The specimens for mechanical testing were prepared using CAD models in SolidWorks, as shown in Figure **2**, and saved in STL format. The STL models were then sliced using CREALITY Print 6 software to generate the G-code required for printing. All specimens were printed using the CREALITY K1C high-speed printer, as shown in Figure **1**(**c**). This printer is specifically designed for high-speed printing of composite materials.

A Universal Testing Machine (UTM), the Testometric M500-25CT (Testometric Co. Ltd., Rochdale, Lancashire, UK), with a maximum load cell capacity of 25 kN, was employed to perform tensile, compressive, and bending tests. ASTM D638-22 Type I was specified with a thickness of 4 mm to print the

Table 3: Parameters maintained as constants during printing

Parameter	Value	Reason
Infill pattern	Gyroid	Excellent for its isotropic properties and energy absorption [12], [15], [16].
Infill density	70%	The Gyroid pattern is, by its very nature, a structure that is not 100% solid.
Nozzle size	0.4 mm	For Hyper-PLA-CF, use the standard from the supplier.
Building orientation	XY (Flat)	For tensile and flexural testing to investigate the intrinsic material strength, and due to the alignment of fibers along the direction of the applied load. [10], [17], [18], [19], [20], [21], [22], [23], [24].
	XZ (Upright)	For the compression testing, the upright was observed to give better results, as the layers were oriented in the transverse direction of the applied load. [16], [22], [25], [26].

Table 4: Taguchi array of Hyper PLA-CF

Run	Layer Thickness (mm)	Inner Wall and Sparse Infill Speed (mm/s)	Nozzle Temperature (˚C)	Building Plate Temperature (˚C)
1	0.1	200	200	50
2	0.1	250	215	60
3	0.1	300	230	70
4	0.2	200	215	70
5	0.2	250	230	50
6	0.2	300	200	60
7	0.3	200	230	60
8	0.3	250	200	70
9	0.3	300	215	50

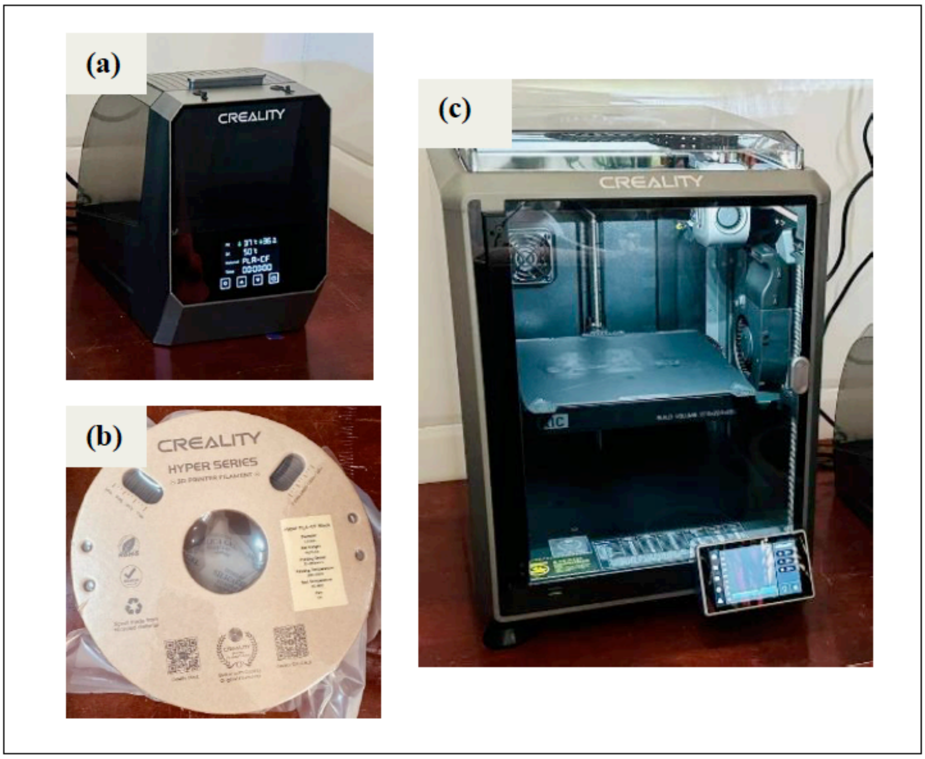

Figure 1: (**a)** CREALITY Dryer, **(b)** Hyper PLA-CF filament, **(c)** CREALITY K1C high-speed printer.

tensile specimens shown in Figure **3**. The tensile test speed was 5 mm/min.

For the compression test, ASTM D695-23 specifies a cylindrical specimen with a 1:2 diameter-to-length ratio, corresponding to the standard specimen size of

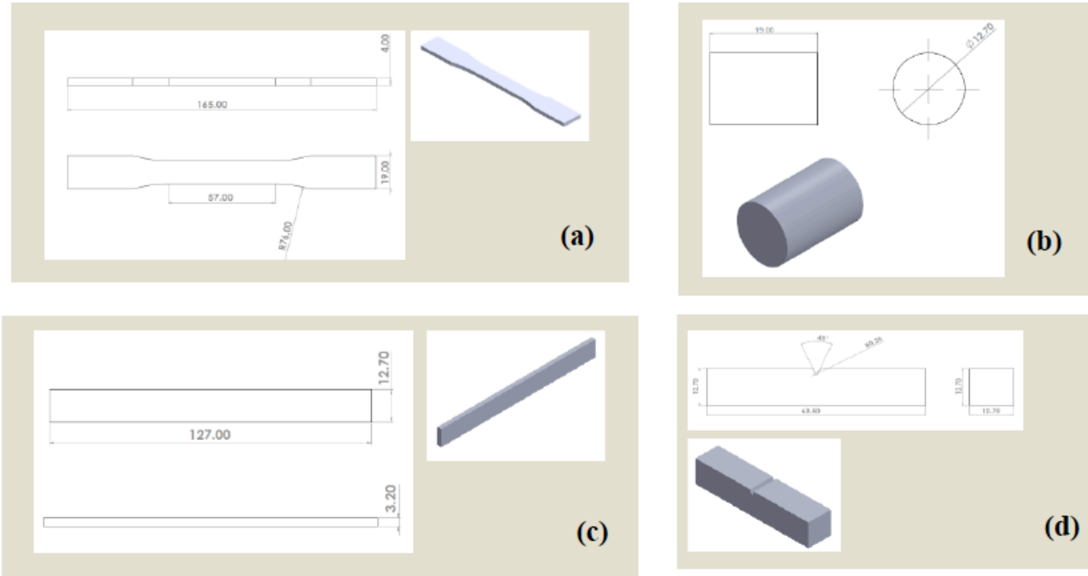

Figure 2: CAD models for the specimens: **(a)** Tensile test according to ASTM (D638-22), **(b)** Compression test following ASTM (D695-23), **(c)** Flexural test as per ASTM (D790), and **(d)** Impact test in accordance with ASTM (D256-23).

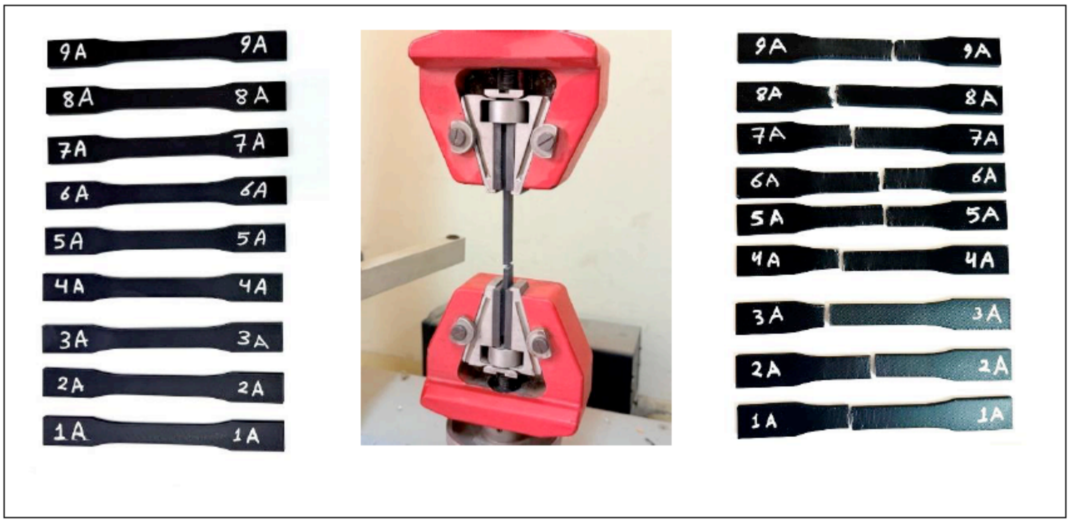

Figure 3: Tensile strength specimens of Hyper PLA-CF prior to, during, and following testing conducted with the Universal Testing Machine.

12.7 mm in diameter and 25.4 mm in length. The specimen exhibited buckling prior to material failure, as illustrated in Figure **4**. To mitigate the effects of slenderness and ensure failure occurred under compression rather than due to structural instability, the specimen length was shortened to prevent buckling, maintaining a diameter-to-length ratio of 1:1.5. The revised geometry was adopted for all compression tests in accordance with the objectives of ASTM D695-23. Consequently, the samples were reprinted at a length of 19 mm and the same diameter of 12.7 mm, as depicted in Figure **5**. The compression test speed was 1.3 mm/min.

Flexural test specimens in ASTM D790 specified rectangular bars measuring 127 mm x 12.7 mm x 3.2 mm. These specimens were printed and then tested using a three-point bending setup with a support span of 100 mm, as illustrated in Figure **6**. The flexural Test Speed was 5.2 mm/min. For the impact test, Method A (Standard Notched Izod) in ASTM D256-23 was specified to test the samples as shown in Figure **7**. The IT 503-IT 504 plastics impact tester was utilized to conduct the test with a pendulum energy of 2.26 J.

Figure 4: Buckling occurred in the compression test sample of 25.4 mm length.

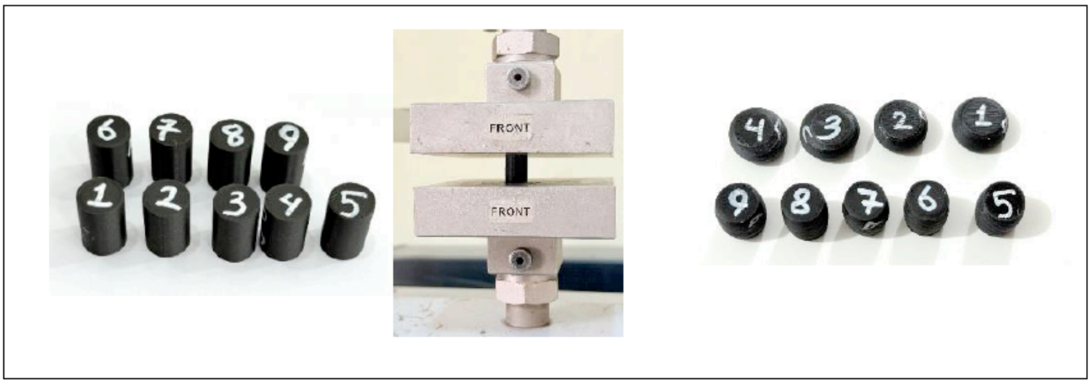

Figure 5: The compression strength samples of Hyper -PLA-CF depicted before, during, and after testing, with the utilization of a universal testing machine.

Figure 6: The bending strength specimens of Hyper PLA-CF before, during, and after testing, as measured by a universal testing machine.

Figure 7: Impact strength specimens of Hyper PLA-CF before, during, and after testing using the IT 503-IT 504 plastics impact tester.

A Scanning Electron Microscopy (SEM) test was conducted to examine the surface morphology of the tensile and bending fracture surfaces. The selected specimens correspond to Taguchi runs 3, 6, and 9 within the experimental design. These three runs represent systematic variations in the primary printing parameters, as summarized in Table **4.** Micrographs were obtained using an Inspect S50 SEM at an accelerating voltage of 30 kV. Each specimen was imaged at three different magnifications to illustrate the various macroscopic and microscopic features of the filament and fiber-matrix interface.

3. RESULTS AND DISCUSSION

Taguchi analysis was employed to evaluate the influence of each printing parameter through signal-to-noise ratio and mean response analysis. Subsequently, empirical mathematical models were independently developed using Multiple Linear

Regression (MLR) based on experimental data from L9 Taguchi array runs. The models incorporated linear, quadratic, and interaction terms, which were iteratively introduced and evaluated according to regression statistics, including the coefficient of determination (R^2), the adjusted coefficient of determination (adjusted R^2), and the predicted coefficient of determination (predicted R^2). The final regression models were selected based on their statistical adequacy and predictive capability rather than being directly derived from the Taguchi orthogonal analysis. For all developed equations, strength outputs are expressed in MPa (tensile, compressive, and bending) or kJ/m^2 (impact). The ranges applicable to these equations are as follows: L (layer thickness) is valid within 0.1-0.3 mm; V (inner wall and sparse infill speed) is over 200–300 mm/s; NT (nozzle temperature) is within 200–230 °C; and BT (build plate temperature) is maintained between 50–70 °C. The subsections elaborate on the results for each mechanical property.

3.1. Tensile Strength

The experimental tensile strength test results are presented in Table **5**, with each trial replicated three times to ensure statistical robustness and minimize experimental variability. Initially, the Taguchi signal-to-noise (S/N) ratio (specifically, the larger-the-better criterion) was employed to identify a robust factor trend influencing the tensile characteristics. The S/N ratio analysis presented in Table **6** indicated that layer thickness is the most influential parameter, exhibiting the largest Delta of 0.59 and ranking first, followed by nozzle temperature. The optimal parameter levels for maximizing tensile performance, derived from the highest mean S/N ratio values in the Taguchi analysis, are detailed in Table **7** and shown visually in Figure **8**, which plots the mean S/N ratio for each parameter level (a main-effects plot), where the it indicates the highest-ranked factor (layer thickness) and the lowest-ranked factor (inner wall & sparse infill speed), visually confirming the ranking reported in Table **6**.

To draw statistically robust conclusions, further analysis was conducted using ANOVA and multiple linear regression in Minitab 22. ANOVA was used to assess the significance of each printing parameter on tensile strength. Consistent with the Taguchi analysis, the ANOVA results in Table **8** confirm that layer thickness is the most influential parameter, with the highest F-value and a significant p-value ($p < 0.001$). A regression model for tensile strength was developed and is shown in Equation 1. Although the build plate temperature ranked third in Taguchi analysis, it has a strong, significant effect ($p = 0.000$) on tensile strength, as shown in Table **8**.

$$T = 142 - 1353\,L + 0.00496\,V - 1.11\,NT + 0.093\,BT - 174.4\,L^2 + 0.00242\,NT^2 + 12.80\,L*NT - 0.0286\,L*NT^2 \quad (1)$$

Where:

T: Tensile Strength

L: Layer thickness

V: Inner wall &sparse infill speed

BT: Build plate Temperature

NT: Nozzle Temperature

Model Summary

S	R-sq	R-sq (adj)	R-sq(pred)
0.473756	88.48%	83.36%	74.08%

It has been observed that the R-sq(pred) value of 74.08 is lower than the R-sq and R-sq(adj) values. This discrepancy is anticipated for tensile strength, which showed the narrowest range of variation among the other responses, and is therefore more sensitive to the small run-to-run experimental scatter inherent in replicate testing. Nevertheless, the R-sq(pred) value remains acceptable, as it exceeds the commonly used threshold of 70%, indicating that the model can still meaningfully predict tensile strength for new observations within specified ranges. Furthermore, the adequacy of the model is corroborated by the S value, representing the residual standard deviation, which is excellent; in addition, the residual plot in Figure **9** demonstrates the adequacy of the model fit, while the scatter plots show points dispersed randomly, indicating that the model assumptions are satisfied.

Figure **10** illustrates the stress-strain curves of tensile strength, providing visual insight into the mechanical behavior. The study emphasizes that layer thickness is a critical factor: thinner layers enhance thermal transfer and fusion between adjacent layers, leading to stronger bonds. Conversely, thicker layers increase the thermal gradient across the interface, which weakens interlayer bonds and accelerates failure. The relatively minor influence of nozzle temperature on tensile strength, in comparison to layer thickness, demonstrates that although nozzle temperature influences melting processes, the contact area and proximity of layer geometry are more significant determinants of interfacial strength. In high-speed printing, limited thermal diffusion highlights the importance of layer geometries. At printing speeds ranging from 200 to 300 mm/s, the window for polymer chain interdiffusion narrows. The finding that layer thickness affects tensile strength more than speed indicates that once a threshold is exceeded, the impact of printing speed becomes minimal; the geometric interface mainly governs tensile performance.

Table 5: Tensile Strength of Experimental Work

Run	Tensile strength 1	Tensile strength 2	Tensile strength 3
1	26.6	26.3	25.9
2	27.8	26.7	27.0
3	27.8	27.6	28.2
4	29.7	30.2	30.7
5	27.8	28.3	28.5
6	29.3	28.6	28.1
7	27.3	28.3	27.9
8	27.2	26.8	26.5
9	27.7	27.1	28.3

Table 7: Optimal Levels Based on Taguchi Analysis of Tensile Strength

Method	Parameter	Optimal Value
Taguchi	Layer thickness	0.2 mm
	Inner wall & sparse infill speed	200 mm/s
	Nozzle temperature	215 °C
	Build plate temperature	70 °C
	Predicted value	**30.2 MPa**
	Confirmation test	**30.7 MPa**

Table 6: Signal-to-Noise Ratios of Tensile Strength

Level	Layer thickness	Inner wall & sparse infill speed	Nozzle Temperature	Build plate Temperature
1	28.65	28.96	28.70	28.75
2	29.25	28.75	29.04	28.90
3	28.77	28.96	28.93	29.02
Delta	0.59	0.21	0.34	0.28
Rank	1	4	2	3

Table 8: Analysis of Variance (ANOVA) of Tensile Strength

Source	DF	Adj SS	Adj MS	F-Value	P-Value
Regression	8	31.0252	3.8781	17.28	0.000
Layer thickness	1	1.3035	1.3035	5.81	0.027
Inner wall &sparse infill speed	1	0.4156	0.4156	1.85	0.190
Nozzle Temperature	1	0.2265	0.2265	1.01	0.328
Build plate Temperature	1	5.8334	5.8334	25.99	0.000
Layer thickness*Layer thickness	1	18.2585	18.2585	81.35	0.000
Nozzle Temperature*Nozzle Temperature	1	0.1976	0.1976	0.88	0.360
Layer thickness*Nozzle Temperature	1	1.3452	1.3452	5.99	0.025
Layer thickness*Nozzle Temperature*Nozzle Temperature	1	1.2459	1.2459	5.55	0.030
Error	18	4.0400	0.2244		
Total	26	35.0652			

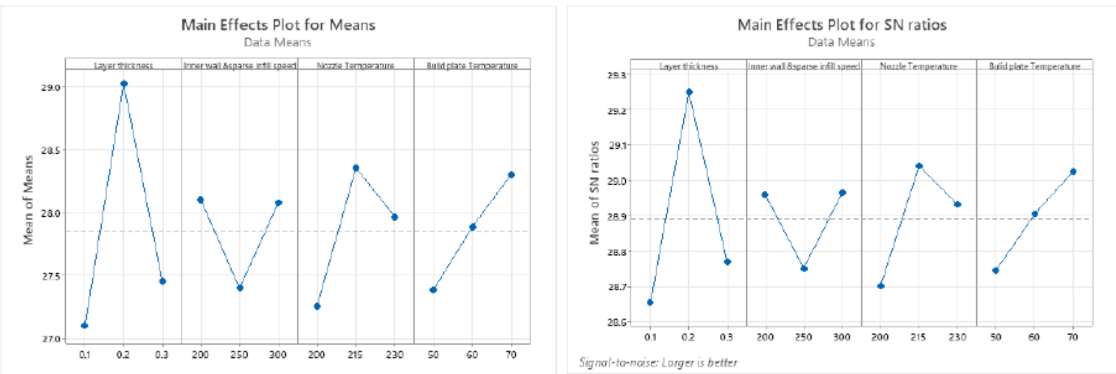

Figure 8: The optimal levels in Taguchi analysis of tensile strength.

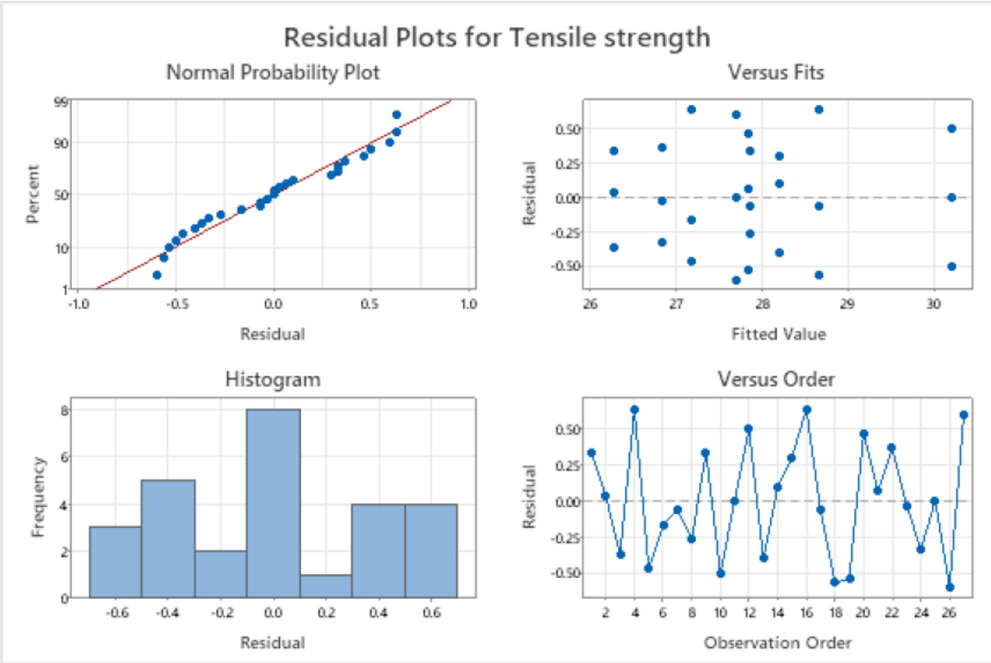

Figure 9: Residuals plot of the model fitting for tensile strength.

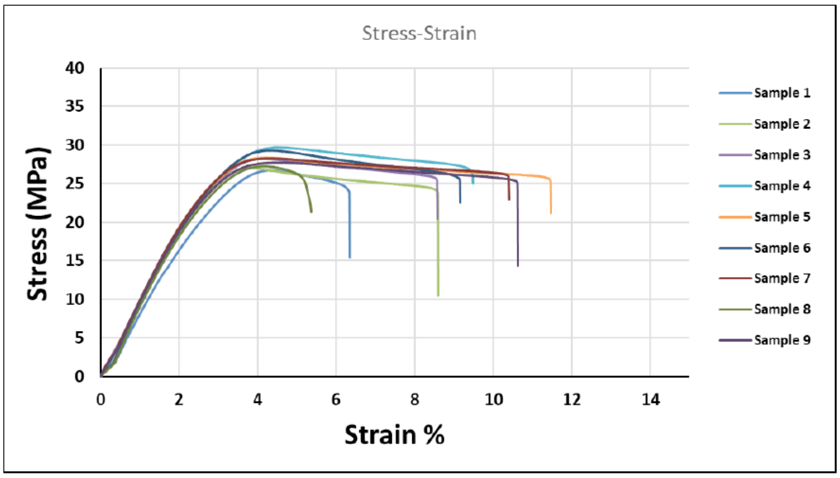

Figure 10: Stress- strain curves of tensile strength of Hyper PLA-CF

3.2. Compression Strength

The experimental results for the compressive tests are detailed in Table **9**. Initial data processing employed the (S/N) ratio to identify the most influential factors. Interestingly, and in contrast to the tensile results, the Build Plate Temperature emerged as the primary driver of the compressive performance, ranking in Table **10** with a delta of 1.9, followed by layer thickness, with a delta of 1.3. The optimal levels for maximizing compression property, based on the highest mean values in the Taguchi analysis, are summarized in Table **12** and shown in Figure **11**, which illustrates the mean compressive strength against each parameter level and demonstrates that the build plate temperature exhibits the steepest and most asymmetric trend, consistent with its top ranking in Table **10**.

ANOVA and multiple linear regression were employed to validate the results and develop a predictive model (Equation 2). Consistent with the Taguchi analysis, the ANOVA results in Table **11** confirm that the build plate temperature is the most significant parameter, with the highest F-value. The residual plot in Figure **12** demonstrates a satisfactory model fit, whereas the scatter plots show points randomly dispersed, thereby validating the model's statistical adequacy. Figure **13** illustrates the stress-strain curve of the compression strength. The build plate temperature crucially affects the compressive strength of components by influencing their thermal history and residual stresses. Precise control improves adherence, reduces warping, and ensures uniform cooling. These factors are vital for maintaining the structural integrity of the internal gyroid infill under compression. The gyroid pattern, recognized for its isotropic characteristics and energy absorption capacity, depends on a stable architecture to prevent buckling [12, 27]. Rapid cooling during high-speed printing can cause thermal stresses, leading to micro-cracks or delamination. Setting an optimal build plate temperature reduces these risks, enhances the part's resistance to compression, and prevents premature buckling, as observed during initial testing.

$$C = -384.0 + 1372\,L - 0.02141\,V + 0.0010\,NT + 14.239\,BT + 208.9\,L^2 - 0.11656\,BT^2 - 47.85\,L*BT + 0.3806\,L*BT^2 \quad (2)$$

Where:

C: Compression Strength

L: Layer thickness

V: Inner wall &sparse infill speed

BT: Build plate Temperature

NT: Nozzle Temperature

Model Summary

S	R-sq	R-sq(adj)	R-sq(pred)
0.540918	98.43%	97.74%	96.48%

Table 9: Compressive strength of Hyper PLA-CF

Run	Compression Strength 1	Compression Strength 2	Compression Strength 3
1	27.5	27.1	28.3
2	34.4	34.7	35.2
3	26.1	26.7	25.8
4	23.5	23.7	22.6
5	26.9	25.3	25.5
6	27.2	26.8	27
7	27	26.9	26.1
8	21.6	21.5	20.8
9	28.2	28.9	27.8

Table 11: Optimal levels based on Taguchi analysis of Compression Strength

Method	Parameter	Optimal value
Taguchi	Layer thickness	0.1 mm
	Inner wall & sparse infill speed	250 mm/s
	Nozzle temperature	215 °C
	Build plate temperature	60 °C
	Predicted value	**34.7 MPa**
	Confirmation test	**33.8 MPa**

Table 10: Signal-to-Noise Ratios of Compression Strength

Level	Layer thickness	Inner wall & sparse infill speed	Nozzle Temperature	Build plate Temperature
1	29.34	28.22	28.01	28.70
2	28.07	28.55	29.06	29.32
3	28.04	28.67	28.38	27.42
Delta	1.30	0.45	1.06	1.90
Rank	2	4	3	1

Table 12: Analysis of Variance (ANOVA) of compression strength

Source	DF	Adj SS	Adj MS	F-Value	P-Value
Regression	8	331.114	41.3893	141.46	0.000
Layer thickness	1	43.657	43.6573	149.21	0.000
Inner wall & sparse infill speed	1	7.733	7.7334	26.43	0.000
Nozzle Temperature	1	0.001	0.0015	0.01	0.944
Build plate Temperature	1	93.264	93.2642	318.75	0.000
Layer thickness*Layer thickness	1	26.181	26.1807	89.48	0.000
Build plate Temperature*Build plate Temperature	1	90.568	90.5680	309.54	0.000
Layer thickness*Build plate Temperature	1	47.372	47.3715	161.90	0.000
Layer thickness*Build plate Temperature*Build plate Temperature	1	43.447	43.4468	148.49	0.000
Error	18	5.267	0.2926		
Total	26	336.381			

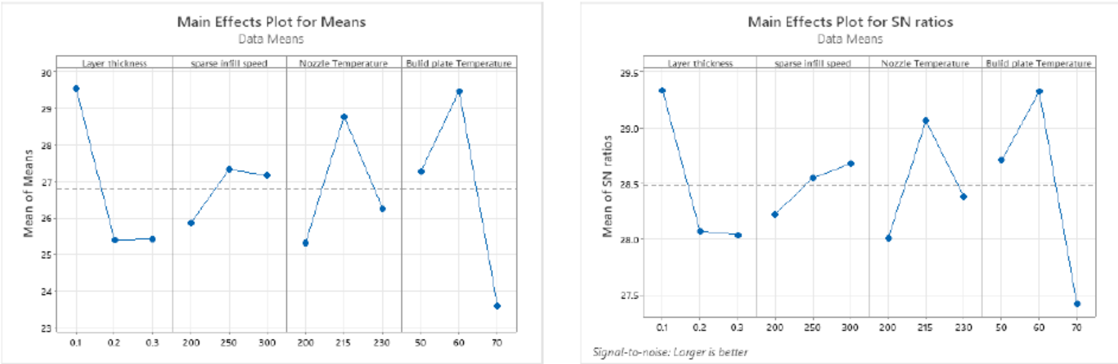

Figure 11: The optimal levels in Taguchi analysis of compression strength.

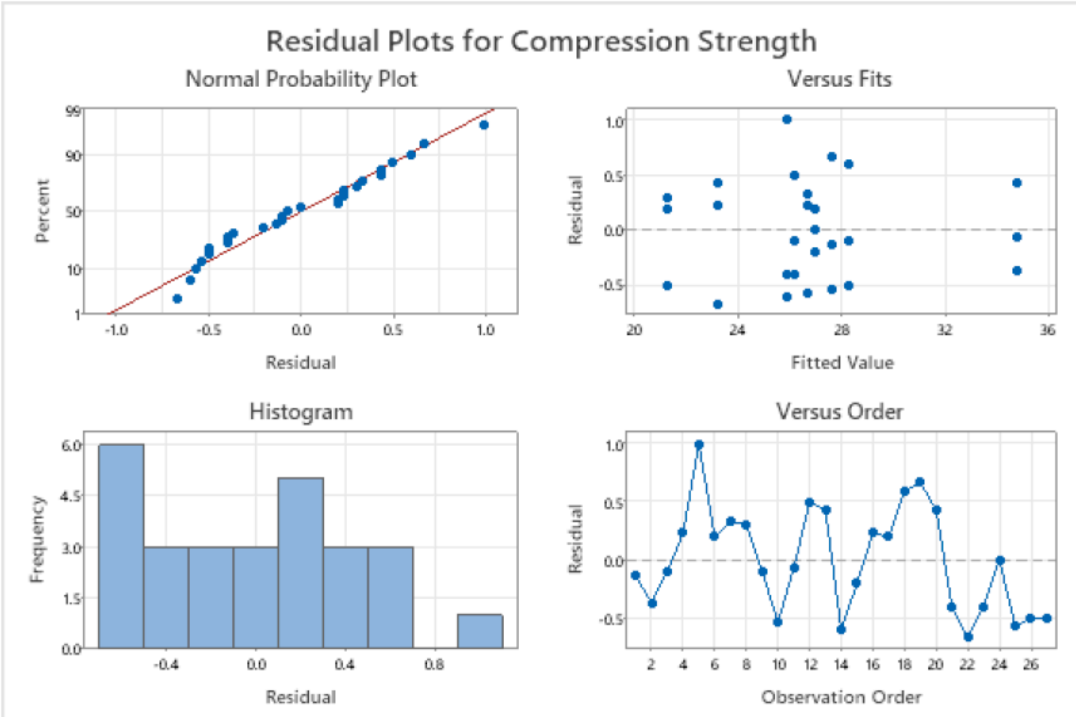

Figure 12: Residuals plot of the model fitted for compressive strength.

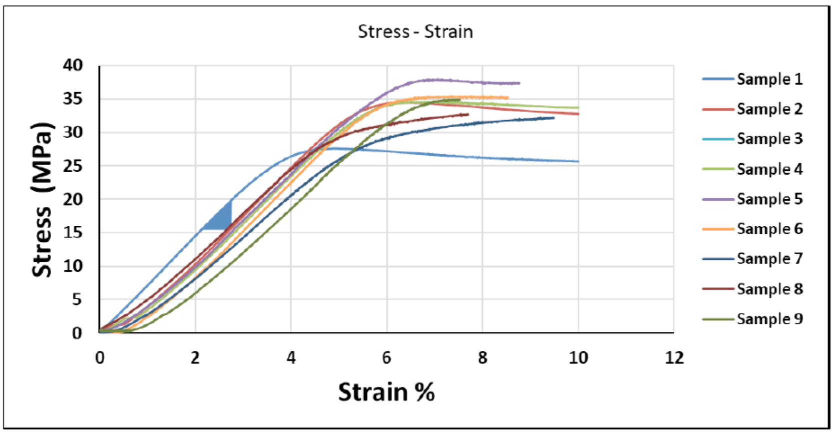

Figure 13: Stress–strain curves illustrating the compressive strength of Hyper PLA-CF.

3.3. Flexural Strength

The flexural strength is provided in Table **13**. The Taguchi analysis indicates that layer thickness is the most influential parameter on flexural strength, with nozzle temperature ranking second, as shown in Table **14**. The optimal levels of printing parameters, identified to maximize flexural performance, are summarized in

Table **15**. Furthermore, Figure **14** presents a main-effects plot showing the mean flexural strength at various parameter levels, with layer thickness exhibiting the most pronounced decreasing trend as thickness increases, consistent with its highest ranking in Table **14**. A predictive model for bending strength is presented in Equation 3, demonstrating its predictive capabilities through R-squared values, with S confirming the model's adequacy. Although Taguchi analysis was prioritized, the ANOVA results in Table **16** demonstrated that printing speed, followed by layer thickness, are the primary factors influencing bending strength, whereas nozzle and build plate temperatures have a less significant impact on the regression model.

Table 13: Bending strength of Hyper PLA-CF

Run	Bending strength 1	Bending strength 2	Bending strength 3
1	61.2	60.7	58.2
2	66.2	63.4	64.3
3	66.8	69.2	67.1
4	59.6	60.4	61.5
5	62.5	61.7	62.3
6	62.2	63	61.9
7	59.8	59.4	58.6
8	47.9	48.3	47.2
9	59.6	57.9	58.4

The residual plot in Figure **15** demonstrates a good fit for the predictive model, and the scatter plots show points randomly dispersed. Figure **16** illustrates the stress-strain curves for bending strength. Printing speed and layer thickness significantly influence thermal diffusion and interlayer interfacial bonding. ANOVA identifies printing speed as the primary determinant of bending strength, contrasting with Taguchi findings. This discrepancy likely reflects the nature of bending loading, where one surface experiences tension while the other undergoes compression, concentrating stress at interlayer interfaces. Consequently, bending strength is particularly sensitive to printing speed.

$$B = -130 - 800.6\,L + 0.088\,V + 2.044\,NT + 0.2111BT - 200\,L^2 - 0.00607\,NT^2 + 3.889\,L * NT \quad (3)$$

Where:

B: Bending Strength

L: Layer thickness

V: Inner wall &sparse infill speed

BT: Build plate Temperature

NT: Nozzle Temperature

Model Summary

S	R-sq	R-sq(adj)	R-sq(pred)
1.01203	97.38%	96.42%	94.97%

Table 15: Optimal levels based on Taguchi analysis of Bending Strength

Method	Parameter	Optimal value
Taguchi	Layer thickness	0.1 mm
	Inner wall & sparse infill speed	300 mm/s
	Nozzle temperature	230 °C
	Build plate temperature	60 °C
	Predicted value	**71.1 MPa**
	Confirmation test	**72.6 MPa**

3.4. Impact Strength

The experimental results of the impact test are presented in Table **17**, with values ranging from 2.17 to 3.45 KJ/m^2. The Taguchi analysis in Table **18** indicates that layer thickness and nozzle temperature are the most significant factors. Thinner layers, such as 0.1 mm, enhance the density of interlayer interfaces. In a notched Izod test, these interfaces act as crack arrestors. A crack propagating through a 0.1 mm layered structure encounters a greater number of interfaces per unit length compared to a 0.3 mm structure, resulting in increased energy dissipation through multiple deformation events and crack deflection pathways. The optimal levels of printing

Table 14: Signal-to-Noise Ratios of Bending Strength

Level	Layer thickness	Inner wall & sparse infill speed	Nozzle Temperature	Build plate Temperature
1	36.13	35.55	35.02	35.60
2	35.80	35.22	35.73	35.85
3	34.80	35.96	35.98	35.28
Delta	1.32	0.73	0.96	0.58
Rank	1	3	2	4

Table 16: Analysis of Variance (ANOVA) of Bending test

Source	DF	Adj SS	Adj MS	F-Value	P-Value
Regression	7	723.367	103.338	100.90	0.000
Layer thickness	1	90.008	90.008	87.88	0.000
Inner wall & sparse infill speed	1	139.392	139.392	136.10	0.000
Nozzle Temperature	1	6.797	6.797	6.64	0.019
Build plate Temperature	1	32.089	32.089	31.33	0.000
Layer thickness*Layer thickness	1	24.000	24.000	23.43	0.000
Nozzle Temperature*Nozzle Temperature	1	11.207	11.207	10.94	0.004
Layer thickness*Nozzle Temperature	1	102.083	102.083	99.67	0.000
Error	19	19.460	1.024		
Lack-of-Fit	1	1.080	1.080	1.06	0.317
Pure Error	18	18.380	1.021		
Total	26	742.827			

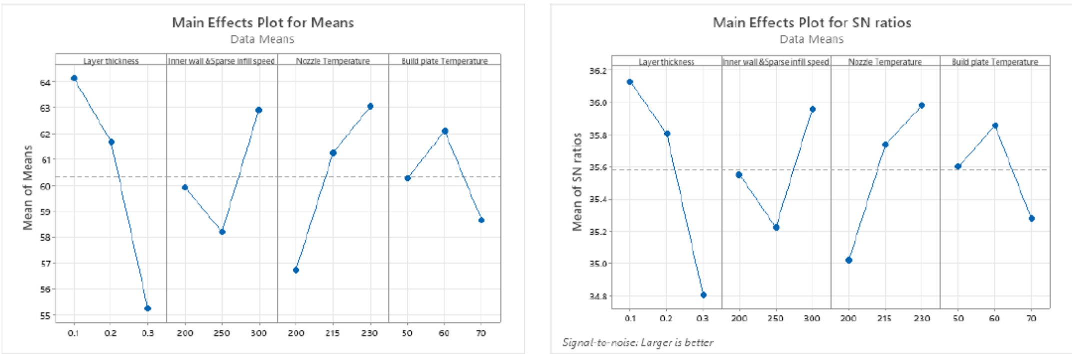

Figure 14: The optimal levels in Taguchi analysis of bending strength.

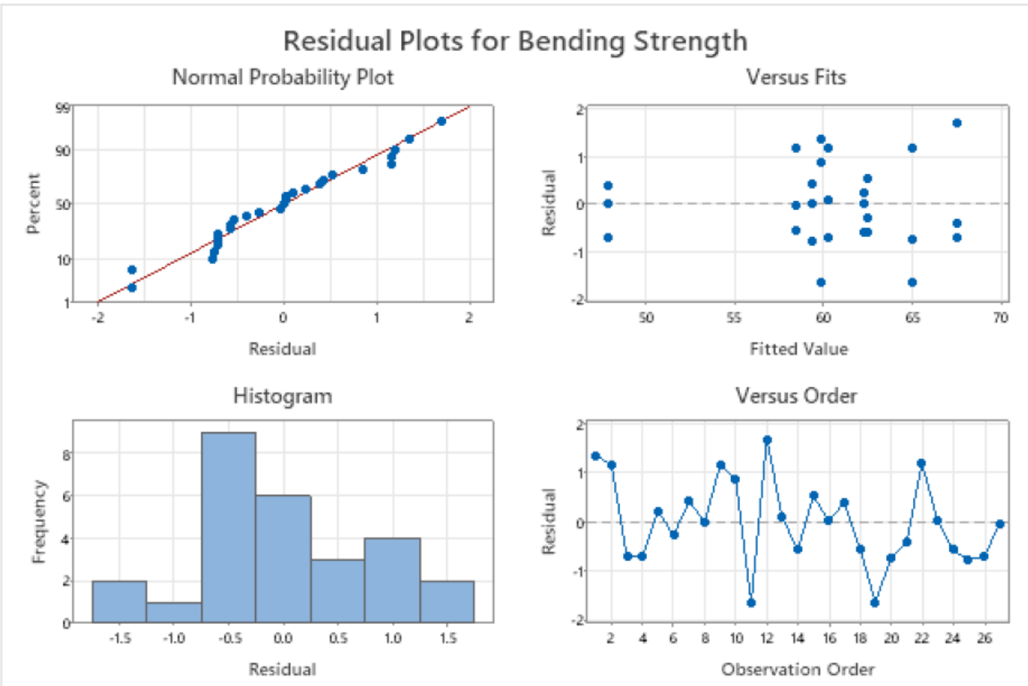

Figure 15: Residuals plot for Hyper PLA-CF bending strength.

parameters are presented in Table **19** and depicted in Figure **17**, illustrating how layer thickness and nozzle temperature exhibit substantial variations relative to the other parameters.

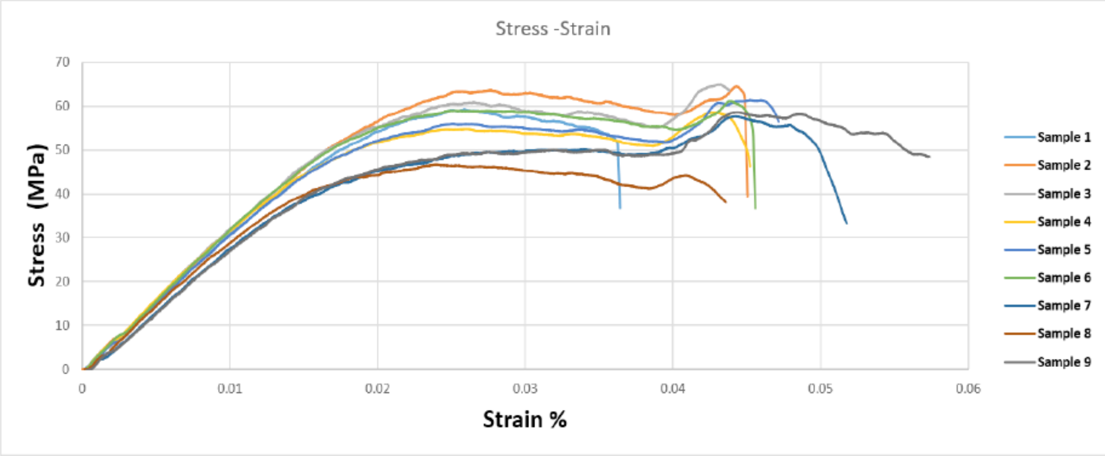

Figure 16: Stress–strain curves for the bending strength of Hyper PLA-CF.

A predictive model was developed as presented in Equation 4. Regarding its predictive capacity, the multiple R-squared values are typical. The ANOVA results indicate a remarkably high F-value for layer thickness as shown in Table **20**, confirming that the geometric configuration of the composite laminate is the primary determinant affecting energy absorption capacity. The residual plot shown in Figure **18** indicates a good fit to the model, and the scatter plots show points randomly dispersed.

$$I = 15.736 - 47.783\,L + 0.002540\,V - 0.001981NT - 0.3133\,BT + 51.149\,L^2 + 0.001963\,BT^2 + 0.4521L * BT \quad (4)$$

Where:

I: Impact Strength

L: Layer thickness

V: Inner wall &sparse infill speed

BT: Build plate Temperature

NT: Nozzle Temperature

Model Summary

S	R-sq	R-sq (adj)	R-sq(pred)
0.0233851	99.75%	99.65%	99.53%

Table 17: Impact strength of experimental work

Run	Impact strength 1 (KJ/m^2)	Impact strength 2 (KJ/m^2)	Impact strength 3 (KJ/m^2)
1	3.061	3.077	3.069
2	2.705	2.697	2.697
3	2.627	2.604	2.612
4	2.341	2.333	2.341
5	2.170	2.178	2.193
6	2.271	2.279	2.263
7	2.441	2.449	2.457
8	3.449	3.441	3.426
9	2.387	2.364	2.379

Table 19: Optimal levels based on Taguchi analysis of Impact Strength

Method	Parameter	Optimal value
Taguchi	Layer thickness	0.1 mm
	Inner wall & sparse infill speed	250 mm/s
	Nozzle temperature	200 °C
	Build plate temperature	70 °C
	Predicted value	**3.478 KJ/m^2**
	Confirmation test	**3.55 KJ/m^2**

Table 18: Signal-to-Noise Ratios of Impact Strength

Level	Layer thickness	Inner wall & sparse infill speed	Nozzle Temperature	Build plate Temperature
1	8.904	8.299	9.197	8.010
2	7.090	8.708	7.840	7.843
3	8.675	7.663	7.632	8.817
Delta	1.814	1.045	1.565	0.974
Rank	1	3	2	4

Table 20: Analysis of Variance (ANOVA) of Impact test results

Source	DF	Adj SS	Adj MS	F-Value	P-Value
Regression	7	4.06749	0.58107	1062.55	0.000
Layer thickness	1	1.55084	1.55084	2835.88	0.000
Inner wall & sparse infill speed	1	0.11616	0.11616	212.41	0.000
Nozzle Temperature	1	0.00636	0.00636	11.63	0.003
Build plate Temperature	1	0.38651	0.38651	706.77	0.000
Layer thickness*Layer thickness	1	1.56972	1.56972	2870.41	0.000
Build plate Temperature*Build plate Temperature	1	0.23125	0.23125	422.87	0.000
Layer thickness*Build plate Temperature	1	0.61314	0.61314	1121.19	0.000
Error	19	0.01039	0.00055		
Lack-of-Fit	1	0.00883	0.00883	101.92	0.000
Pure Error	18	0.00156	0.00009		
Total	26	4.07788			

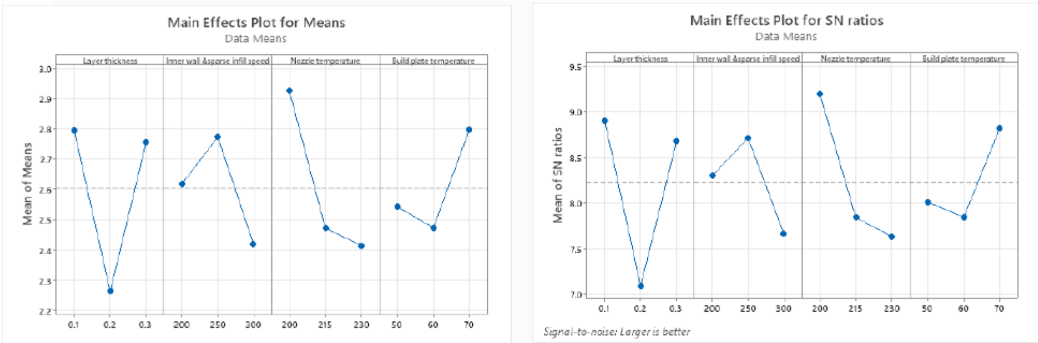

Figure 17: The optimal levels in Taguchi analysis of Impact strength.

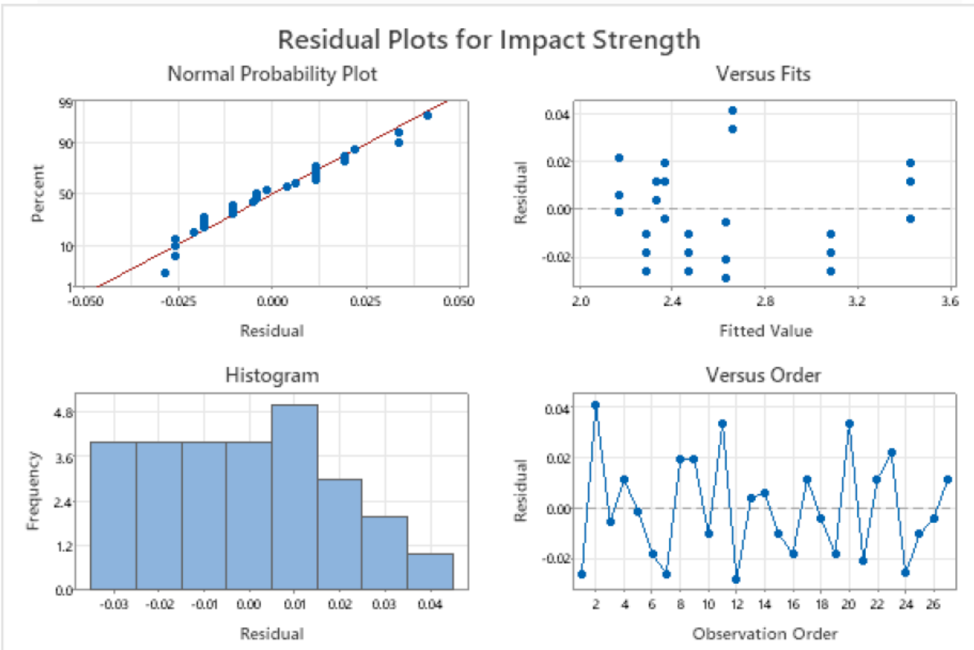

Figure 18: Residuals plot of Hyper PLA-CF for Impact Strength.

3.5. Microstructural Observations of the SEM Assessment

To investigate the microstructure of the composite materials and understand the effect of printing parameters on the structure, SEM tests have been conducted on the fracture surfaces of tensile and flexural samples from Hyper PLA-CF specimens. The samples inspected have been selected at three levels, each maintaining the same printing speed of 300 mm/s but differing in layer thickness, nozzle temperature, and build plate temperature.

3.5.1. Flexural Fracture Surface Morphology of Hyper PLA-CF

The flexural fracture surface of Hyper PLA-CF sample 3 (L=0.1 mm, NT=230 C, BT= 70), shown in Figure **19**(**a**), displays a complex morphology influenced by layer thickness and nozzle temperature, affecting interlayer bonding and fracture behavior. It exhibits the roughest, most intricate fracture, indicating superior interfacial bonding and energy absorption. The thin layers and high nozzle temperature enhanced interdiffusion, promoting good consolidation, as seen by red lines. The gyroid strut showed irregular boundaries, reflecting improved plastic flow during deposition. Higher magnification reveals extensive fusion zones and limited incomplete adhesion. Fiber pull-out, indicated by blue arrows, suggests fiber-matrix debonding as the main energy dissipation during fracture. Small voids were present but did not dominate failure. These characteristics align with the highest observed flexural strength among the examined specimens.

Sample 6 (L=0.2 mm, NT=200°C, BT=60°C), shown in Figure **19**(**b**), exhibited weaker interlayer adhesion than sample 3, with the gyroid beads preserving a regular morphology, thereby indicating limited polymer flow at the lower nozzle temperature. Partial separation suggested incomplete consolidation, and the fracture surfaces appeared smoother with reduced fibre pull-out compared to Sample 3, implying decreased ductility and energy absorption capability. Cracks propagated more readily at interfaces, thereby diminishing the bending strength.

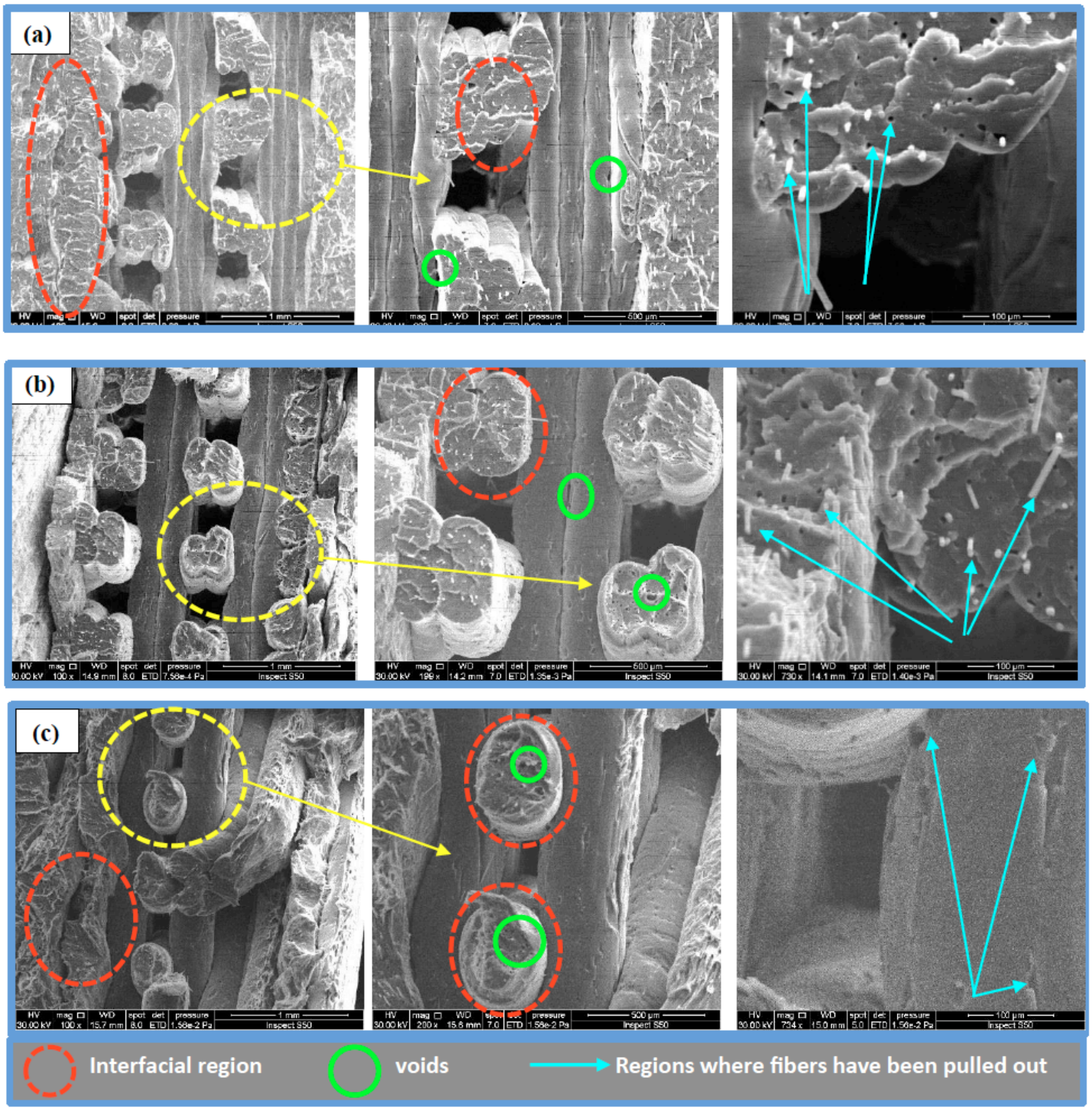

Figure 19: SEM micrographs of Hyper PLA-CF flexural fracture surfaces at different magnifications **(a)** Sample 3 (L=0.1 mm, NT=230°C, BT=70°C); **(b)** Sample 6 (L=0.2 mm, NT=200°C, BPT=60°C); **(c)** Sample 9 (L=0.3 mm, NT=215°C, BPT=50°C).

The interfacial degradation is clearly demonstrated in sample 9 (L=0.3 mm, NT=215°C, BT=50°C), as shown in Figure **19**(**c**). The thickest layer, with the lowest build plate temperature, exhibited extensive delamination and reduced adhesion between the shell and the gyroid structure. The beads of the gyroid pattern maintained their original geometry after fracture, indicating failure due to weak interlayer bonding. The fracture surface was smooth, with minimal fibre pull-out observed, alongside large voids. This phenomenon is attributable to insufficient consolidation and inadequate melt compaction, which also results in decreased energy absorption and aligns with the lowest flexural strength observed in the data set. Furthermore, it is consistent with the layer thickness identified as the most influential parameter in the Taguchi analysis.

3.5.2. Tensile Fracture Surface Morphology of Hyper PLA-CF

The fracture surface of tensile specimens subjected to tensile testing has exhibited trends consistent with those observed under flexural loading, referencing the predominant influence of layer thickness and processing temperatures on the strength of interlayer bonding and mechanical behavior. However, unlike flexural loading, where tensile and compressive stresses act concurrently, in tensile loading, crack propagation initiates directly through the weak interfacial regions aligned with the loading direction.

Sample 3, as illustrated in Figure **20**(**a**), displayed a rough fracture surface characterized by a high occurrence of fiber pull-out and matrix tearing. Elevated nozzle temperature improved polymer

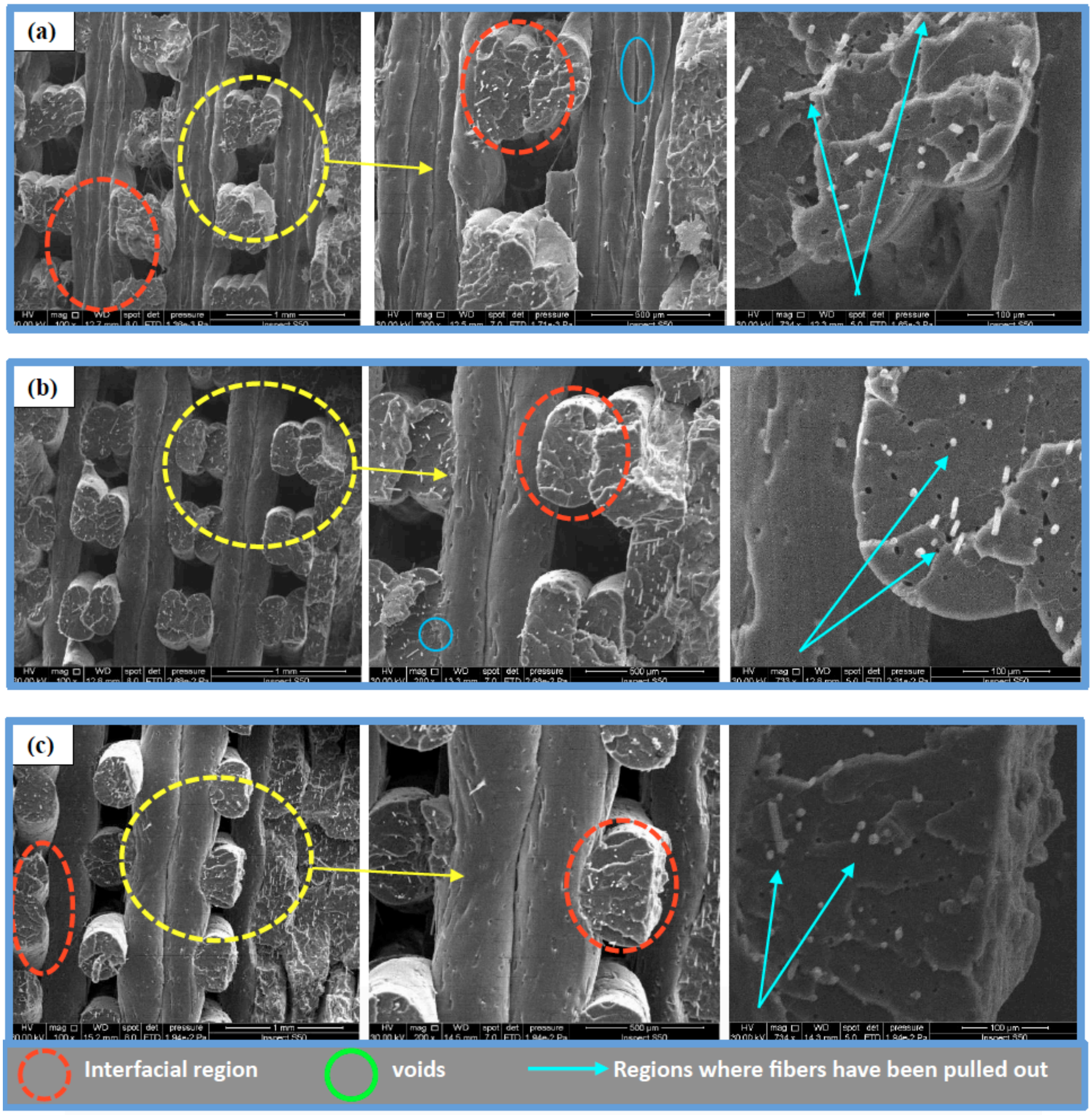

Figure 20: SEM micrographs of Hyper PLA-CF tensile fracture surfaces at different magnifications **(a)** Sample 3 (L=0.1 mm, NT=230°C, BT=70°C); **(b)** Sample 6 (L=0.2 mm, NT=200°C, BPT=60°C); **(c)** Sample 9 (L=0.3 mm, NT=215°C, BPT=50°C).

interdiffusion, while the thinnest layer thickness contributed to the formation of additional interfacial bonds throughout the sample's depth. Although localized voids and shell-infill gaps persisted, the fracture morphology suggested relatively strong interlayer adhesion and marked resistance to crack propagation.

Sample 6, as depicted in Figure **20**(**b**), exhibited an intermediate fracture response. The regular geometry of the beads was observed, with limited fiber fracture and smoother matrix regions. Moderate interfacial bonding and a mixed adhesive-cohesive failure mode were identified, which explains the intermediate tensile performance.

Sample 9, depicted in Figure **20**(**c**), exhibits extensive interlayer delamination. The decreased fiber pull-out, combined with preserved strut geometry, suggests an adhesive fracture failure, indicative of inadequate consolidation between layers. The thickest layer, measuring 0.3 mm, resulted in reduced interdiffusion and fewer bonding interfaces, which explains the lower tensile performance observed in this specimen.

3.6. Conclusions and Future Work

This study offers a detailed mechanical evaluation of Hyper PLA-CF, tailored for high-speed FFF printing, a critical area for the industrial adoption of additive manufacturing. Tensile, compression, bending, and impact tests were performed utilizing the Taguchi method to structure the experimental procedures. Taguchi, multiple linear regression and ANOVA analyses were applied to analyze the data, emphasizing the optimal levels of printing parameters and evaluating the significance of each parameter's contribution to the output characteristics. The findings illustrated the following:

Layer thickness is key for tensile, bending, and impact loads, while thermal management of the build plate temperature is vital for compressive loads. Regression shows significant interactions in tensile strength between layer thickness and nozzle temperature, and in bending strength between layer thickness and build plate temperature for compression.

Figure **21** shows the average mechanical responses across four loading modes as a function of printing parameters, highlighting how processing conditions affect material properties. Layer thickness significantly impacts properties: increasing thickness reduces bending strength but raises impact strength. Thinner layers improve interfacial density and stiffness but may lower energy absorption. Tensile and compressive strengths stay consistent, indicating geometric factors dominate in bending and impact tests. The nozzle temperature has a moderate effect; responses in bending, impact, and tensile tests are less sensitive, aligning with Taguchi results. The build plate temperature primarily affects compression strength, highlighting the role of thermal management in stabilizing the gyroid infill. Higher substrate temperatures increase bending strength but decrease impact strength, signaling a stiffer, less tough interface. Inner wall and infill printing speeds (200-300 mm/s) have minimal influence because material rheology compensates for thermal diffusion, making geometry and temperature more critical.

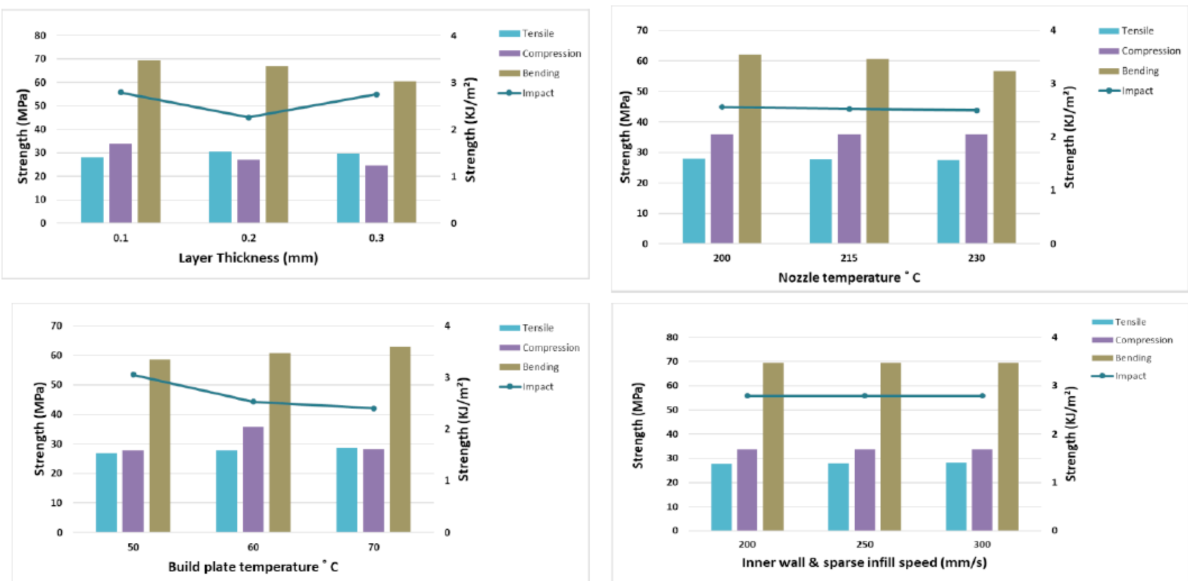

Figure 21: The influence of printing parameters on the mechanical properties of hyper PLA-CF fabricated via high-speed FDM, including tensile strength, compressive strength, bending strength (measured in MPa), and impact strength (measured in kJ/m²).

The SEM observations substantiate the statistical findings from the Taguchi and ANOVA analyses. The primary influencing parameters are layer thickness and nozzle temperature: an increase in layer thickness leads to delamination, and an increase in nozzle temperature promotes interdiffusion and consolidation of neighboring layers.

Future studies may apply multi-objective optimization to help balance tensile, compressive, bending, and impact requirements of complex parts, thereby promoting high-speed FFF in advanced manufacturing.

CREDIT AUTHORSHIP CONTRIBUTION STATEMENT

Roaa H. Ibrahim: Conceptualization, Methodology, Software, Experimental work, Writing- Original Draft, Writing- review & editing, Visualization.

Hala Salman: Conceptualization, Methodology, Experimental work, Writing– original draft, Review & Editing, Supervision, Project administration, Visualization.

All authors have reviewed and approved the final version of the manuscript.

FUNDING STATEMENT

This study received no specific financial support from public, commercial, or nonprofit agencies.

DECLARATION OF INTERESTS

The authors declare that they have no known conflicts of interest, whether financial or personal, that could have influenced the work reported in this paper.

REFERENCES

[1] D. K. Mishra, J. Giri, T. Sathish, M. Kanan, and D. Prajapati, "Influence of 3D printing process parameters on mechanical properties of PLA based ceramic composite parts," Results in Engineering, vol. 25, p. 104488, Mar. 2025, https://doi.org/10.1016/j.rineng.2025.104488

[2] H. B. Ali *et al.*, "Experimental Mechanical Property Investigation on PLA-CF Specimens using Fused Filament Fabrication Technology," Eng. Technol. Appl. Sci. Res., vol. 15, no. 3, pp. 23995–24004, Jun. 2025, https://doi.org/10.48084/etasr.10111

[3] N. Maqsood and M. Rimašauskas, "Characterization of carbon fiber reinforced PLA composites manufactured by fused deposition modeling," Composites Part C: Open Access, vol. 4, p. 100112, Mar. 2021, https://doi.org/10.1016/j.jcomc.2021.100112

[4] M. Cao *et al.*, "Investigation of Carbon Fiber on the Tensile Property of FDM-Produced PLA Specimen," Polymers, vol. 14, no. 23, p. 5230, Dec. 2022, https://doi.org/10.3390/polym14235230

[5] A. Farzipour and R. Hasanzadeh, "On the impact of ultra-high printing speeds on tensile efficiency of fused filament fabrication-3D printed polylactic acid," Rapid Prototyping Journal, pp. 1–11, Dec. 2025, https://doi.org/10.1108/RPJ-08-2025-0359

[6] B. B. Fraj and Z. Ahmed, "Thermal, Structural, and Mechanical Properties of Carbon Fiber Reinforced PLA Composites: Influence of FDM Print Speed and Comprehensive Analysis," Polymer Composites, vol. 46, no. 18, pp. 17229–17239, Dec. 2025, https://doi.org/10.1002/pc.70107

[7] E. Vălean, L. Marșavina, S.-V. Galațanu, P. Foti, and F. Berto, "Are carbon fibres beneficial to improve mechanical and fracture properties of FDM printed composites?," Engineering Fracture Mechanics, vol. 332, p. 111791, Feb. 2026, https://doi.org/10.1016/j.engfracmech.2025.111791

[8] R. H. Ibrahim and H. Salman, "Manufacturing of polymer-based composite material by FDM: challenges and opportunities for functional parts design," Next Materials, vol. 10, p. 101571, Jan. 2026, https://doi.org/10.1016/j.nxmate.2025.101571

[9] A. Wang, X. Tang, Y. Zeng, L. Zou, F. Bai, and C. Chen, "Carbon Fiber-Reinforced PLA Composite for Fused Deposition Modeling 3D Printing," Polymers, vol. 16, no. 15, p. 2135, Jul. 2024, https://doi.org/10.3390/polym16152135

[10] M. Kamaal, M. Anas, H. Rastogi, N. Bhardwaj, and A. Rahaman, "Effect of FDM process parameters on mechanical properties of 3D-printed carbon fibre–PLA composite," Prog Addit Manuf, vol. 6, no. 1, pp. 63–69, Feb. 2021, https://doi.org/10.1007/s40964-020-00145-3

[11] B. Blake, R. Mendenhall, and B. Eslami, "Balancing Strength and Flexibility: Mechanical Characterization of Carbon Fiber-Reinforced PLA Composites in FDM 3D Printing," JMMP, vol. 9, no. 9, p. 288, Aug. 2025, https://doi.org/10.3390/jmmp9090288

[12] R. Kumaresan, M. T. Pandurangan, and K. Kanny, "Mechanical and microstructural behavior of FDM-Printed Hyper-PLA by optimizing process parameters," Int J Adv Manuf Technol, Feb. 2026, https://doi.org/10.1007/s00170-026-17686-6

[13] J. Bochnia, M. Blasiak, and T. Kozior, "A Comparative Study of the Mechanical Properties of FDM 3D Prints Made of PLA and Carbon Fiber-Reinforced PLA for Thin-Walled Applications," Materials, vol. 14, no. 22, p. 7062, Nov. 2021, https://doi.org/10.3390/ma14227062

[14] O. Araque, L. A. Sánchez-Echeverri, and I. X. Cerón, "Impact of Printing Angle and Layer Height on the Mechanical Strength of PLA Reinforced with Chopped Carbon Fibres Using FDM 3D Printing," Polymers, vol. 17, no. 22, p. 3069, Nov. 2025, https://doi.org/10.3390/polym17223069

[15] R. Spina, L. Morfini, and L. M. Galantucci, "Mechanical properties of lightweight 3D-printed structures made with carbon-filled nylon," Prog. Addit. Manuf., vol. 9, no. 6, pp. 2483–2497, 2024, https://doi.org/10.1007/s40964-024-00595-z

[16] D. K. Yadav, R. Srivastava, and S. Dev, "Design & fabrication of ABS part by FDM for automobile application," Materials Today: Proceedings, vol. 26, pp. 2089–2093, 2020, https://doi.org/10.1016/j.matpr.2020.02.451

[17] O. K. Arigbabowo and J. S. Tate, "Additive manufacturing of polyamide nanocomposites for electrostatic charge dissipation applications," Materials Science and Engineering: B, vol. 271, p. 115251, Sep. 2021, https://doi.org/10.1016/j.mseb.2021.115251

[18] S. Dul, L. Fambri, and A. Pegoretti, "High-Performance Polyamide/Carbon Fiber Composites for Fused Filament Fabrication: Mechanical and Functional Performances," J. of Materi Eng and Perform, vol. 30, no. 7, pp. 5066–5085, Jul. 2021, https://doi.org/10.1007/s11665-021-05635-1

[19] J. M. Chacón, M. A. Caminero, P. J. Núñez, E. García-Plaza, I. García-Moreno, and J. M. Reverte, "Additive manufacturing of continuous fibre reinforced thermoplastic composites using fused deposition modelling: Effect of process

parameters on mechanical properties," Composites Science and Technology, vol. 181, p. 107688, Sep. 2019, https://doi.org/10.1016/j.compscitech.2019.107688

[20] B. A. Ahmed *et al*., "Printing Parameter Optimization of Additive Manufactured PLA Using Taguchi Design of Experiment," Polymers, vol. 15, no. 22, p. 4370, Nov. 2023, https://doi.org/10.3390/polym15224370

[21] H. H. Abdulridha and T. F. Abbas, "Analysis and Investigation the Effect of the Printing Parameters on the Mechanical and Physical Properties of PLA Parts Fabricated via FDM Printing," Adv. Sci. Technol. Res. J., vol. 17, no. 6, pp. 49–62, Dec. 2023, https://doi.org/10.12913/22998624/173562

[22] L. K. John, R. Murugan, and S. Singamneni, "Impact of quasi-isotropic raster layup on the mechanical behaviour of fused filament fabrication parts," High Performance Polymers, vol. 34, no. 1, pp. 77–86, Feb. 2022, https://doi.org/10.1177/09540083211041954

[23] A. Zotti, T. Paduano, F. Napolitano, S. Zuppolini, M. Zarrelli, and A. Borriello, "Fused Deposition Modeling of Polymer Composites: Development, Properties and Applications," Polymers, vol. 17, no. 8, p. 1054, Apr. 2025, https://doi.org/10.3390/polym17081054

[24] M. Graba and A. Grycz, "Assessment of the Mechanical Properties of Selected PLA Filaments Used in the UAV Project," Materials, vol. 16, no. 3, p. 1194, Jan. 2023, https://doi.org/10.3390/ma16031194

[25] I. Hager *et al*., "Interlayer Bond Strength Testing in 3D-Printed Mineral Materials for Construction Applications," Materials, vol. 15, no. 12, p. 4112, Jun. 2022, https://doi.org/10.3390/ma15124112

[26] A. Gebisa and H. Lemu, "Investigating Effects of Fused-Deposition Modeling (FDM) Processing Parameters on Flexural Properties of ULTEM 9085 using Designed Experiment," Materials, vol. 11, no. 4, p. 500, Mar. 2018, https://doi.org/10.3390/ma11040500

[27] B. A. Ahmed *et al*., "Printing Parameter Optimization of Additive Manufactured PLA Using Taguchi Design of Experiment," Polymers, vol. 15, no. 22, p. 4370, Nov. 2023, https://doi.org/10.3390/polym15224370

https://doi.org/10.12974/2311-8717.2026.14.06